



HAL
open science

Impact of an Artificial Digestion Procedure on Aluminum-Containing Nanomaterials

Holger Sieg, Claudia Kästner, Benjamin Krause, Thomas Meyer, Agnès Burel,
Linda Böhmert, Dajana Lichtenstein, Harald Jungnickel, Jutta Tentschert,
Peter Laux, et al.

► **To cite this version:**

Holger Sieg, Claudia Kästner, Benjamin Krause, Thomas Meyer, Agnès Burel, et al.. Impact of an Artificial Digestion Procedure on Aluminum-Containing Nanomaterials. *Langmuir*, 2017, 33 (40), pp.10726-10735. 10.1021/acs.langmuir.7b02729 . hal-01617104

HAL Id: hal-01617104

<https://univ-rennes.hal.science/hal-01617104>

Submitted on 16 Oct 2017

HAL is a multi-disciplinary open access archive for the deposit and dissemination of scientific research documents, whether they are published or not. The documents may come from teaching and research institutions in France or abroad, or from public or private research centers.

L'archive ouverte pluridisciplinaire **HAL**, est destinée au dépôt et à la diffusion de documents scientifiques de niveau recherche, publiés ou non, émanant des établissements d'enseignement et de recherche français ou étrangers, des laboratoires publics ou privés.

Impact of an artificial digestion procedure on aluminum-containing nanomaterials

Holger Sieg¹, Claudia Kästner³, Benjamin Krause², Thomas Meyer⁴, Agnès Burel⁵, Linda Böhmert¹, Dajana Lichtenstein¹, Harald Jungnickel², Jutta Tentschert², Peter Laux², Albert Braeuning¹, Irina Estrela-Lopis⁴, Fabienne Gauffre⁵, Valérie Fessard⁶, Jan Meijer⁷, Andreas Luch², Andreas F. Thünemann³ and Alfonso Lampen¹

¹ German Federal Institute for Risk Assessment, Max-Dohrn-Straße 8-10, 10589 Berlin, Department of Food Safety

² German Federal Institute for Risk Assessment, Max-Dohrn-Straße 8-10, 10589 Berlin, Department of Chemical and Product Safety

³ Bundesanstalt für Materialforschung und -prüfung (BAM), Unter den Eichen 87, 12205 Berlin

⁴ Institute of Medical Physics and Biophysics, Leipzig University, Härtelstrasse 16-18, 04275 Leipzig, Germany

⁵ Institut des Sciences Chimiques de Rennes, UMR-CNRS 6226, Université de Rennes 1, France

⁶ ANSES, French Agency for Food, Environmental and Occupational Health and Safety, Fougères Laboratory, Toxicology of contaminants unit, 10B rue Claude Bourgelat, 35306, Fougères Cedex, France

⁷ Felix Bloch Institute for Solid State Physics, Leipzig University, Linnéstraße 5, 04103 Leipzig, Germany

Corresponding author

Linda.Boehmert@bfr.bund.de

Tel.: +49 30 18412 2042

Keywords

nanoparticles, aluminum, artificial digestion, gastrointestinal tract, agglomeration, ion release, *de novo* emerging of particles

Abstract

Aluminum has gathered toxicological attention due to human exposure and its suspected hazardous potential. Nanoparticles from food supplements or food contact materials may reach the human gastrointestinal tract. Here, we investigated the physico-chemical fate of aluminum-containing nanoparticles and aluminum ions during *in vitro*-digestion throughout the main stages of the human gastrointestinal tract.

Small-angle X-ray scattering (SAXS), transmission electron microscopy (TEM), ion beam microscopy (IBM), secondary ion beam mass spectrometry (TOF-SIMS), and inductively coupled plasma mass spectrometry (ICP-MS) in the single-particle mode were employed to characterize two aluminum-containing nanomaterials with different particle core materials (Al^0 , $\gamma\text{Al}_2\text{O}_3$) and soluble AlCl_3 .

Particle size and shape remained unchanged in saliva, whereas strong agglomeration of both aluminum nanoparticle species was observed at low pH in gastric fluid together with an increased ion release. The levels of free aluminum ions decreased in intestinal fluid and the particles de-agglomerated, thus liberating primary particles again. Dissolution of nanoparticles was limited and substantial changes of their shape and size were not detected. The amounts of particle-associated phosphorus, chlorine, potassium and calcium increased in intestinal fluid, as compared to nanoparticles in standard dispersion. Interestingly, nanoparticles were found in the intestinal fluid after addition of ionic aluminum.

We provide a comprehensive characterization of the fate of aluminum nanoparticles in the simulated gastrointestinal fluids, demonstrating that orally ingested nanoparticles probably reach the intestinal epithelium. The balance between dissolution and *de novo* complex formation should be considered when evaluating nanotoxicological experiments.

Introduction

Aluminum is the most common metal in the biosphere and therefore ubiquitous present in food and consumer products ¹. However, no essential physiological role of aluminum is known, possibly due to its inflexible trivalent oxidation state and its relatively low reactivity ²⁻³. Most aluminum on earth is bound in minerals that are in a chemically inactive state ⁴. In the last two centuries more and more aluminum was transferred into the metallic and in the more reactive ionic form, due to industrial activities and acidification of the environment ⁵⁻⁶. Activation seems to be triggered by acidic pH ⁴. Chronic exposure to aluminum can be harmful for certain groups of people, for example for those with renal dysfunction ⁷. The suspected hazardous potential of aluminum on human health recently led to an increasing attentiveness on this topic, as a correlation between the use of aluminum-containing products and Alzheimer's disease or breast cancer has been proposed ⁸⁻⁹.

Oral ingestion is an important uptake route for aluminum. Exposure might result from natural sources, such as drinking water, but also from food additives, packaging and kitchenware ³. The use of aluminum-containing packaging, consumer products and kitchenware has increased ¹⁰, as well as the use of chemical solvents, leaches and acids. Several metal species are present in a significant amount in food as nano-scaled particles ¹¹⁻¹² and migrate into food from packaging material ¹³⁻¹⁵. Like other orally ingested metals, aluminum nanoparticles overcome the different compartments of the human digestion tract. During this process, the chemical environment changes severely from mouth to stomach and intestine with regard to shifts in pH and the presence of complex mixture of salts, proteins and intestinal bile acids with surface-active properties. These changes may induce nanoparticle modifications including dissolution, agglomeration and deagglomeration and so affect intestinal uptake which differs significantly between dissolved ions and nanoparticles depending on their size, shape and physicochemical properties ¹⁶. These properties include surface coating, protein corona composition, and biological environment ¹⁷. Therefore, it is crucial to characterize nanoparticles under realistic conditions.

To mimic these conditions, different modifications of physiologically buffered fluids have been applied in research, with some of them using buffered solutions with only pH changes ¹⁸, whilst others use more complex systems which include salts, digestion enzymes, proteins or other food components ¹⁹⁻²⁰. Moreover, such models with higher complexity are appropriate to observe changes in the physicochemical characteristics of metallic nanoparticles and also enable detailed studies on the toxicological potential of particles following intestinal digestion ²¹.

The chemical identity of aluminum is an important factor for its toxicological potential. This study focuses on the fate and behavior of different aluminum species during the digestion

1
2
3 process after oral uptake. Therefore, three different aluminum species were used which
4 represent soluble ionic Aluminum (AlCl_3), elementary metallic aluminum (Al^0) and mineral
5 oxidized aluminum (Al_2O_3). These three representative aluminum entities were analyzed
6 separately in a complex artificial digestion system consisting of three steps, namely saliva,
7 gastric juice, and intestinal juice. Differences in ionic content, particle size, shape, element
8 attachment, agglomeration state and stability were investigated using elemental analysis,
9 small angle x-ray scattering (SAXS), transmission electron microscopy (TEM), single particle
10 inductively coupled plasma mass spectrometry (SP-ICP-MS), ion beam microscopy (IBM)
11 and time of flight secondary ion mass spectrometry (ToF-SIMS).
12
13
14
15
16
17
18

19 **Experimental Section**

20 Chemicals and nanoparticles

21
22
23 Chemicals were purchased from Sigma-Aldrich (Taufkirchen, Germany), Merck (Darmstadt,
24 Germany), or Carl Roth (Karlsruhe, Germany) in the highest available purity.
25

26
27 Nanomaterials (Al^0 -core surface-passivated nanoparticles and $\gamma\text{-Al}_2\text{O}_3$ nanoparticles) were
28 supplied by IoLiTec. Al^0 nanoparticles were stored and weighted under an argon
29 atmosphere. Both particles were freshly dispersed at a concentration of 2.56 mg/ml
30 according to the modified NanoGenoTOX protocol (ultrasonication applying an energy of
31 1176 kJ/ml dispersion using an acoustic power of 7.35 W), stabilized by 0.05% BSA/water
32 before use. BSA was supplied by Carl Roth (Albumin Fraction V, $\geq 98\%$) and AlCl_3 was
33 supplied by Sigma Aldrich (Hexahydrate, $\geq 97\%$).
34
35
36
37
38
39

40 Artificial *in vitro* digestion

41
42 Artificial *in vitro* digestion was originally based on DIN ISO 19738 and distinctly modified for
43 scientific investigations on metals, metallic nanoparticles¹⁹⁻²⁴, and other nanoparticles and
44 biopolymers²⁵⁻²⁶. As described in Figure 1, the artificial *in vitro* digestion consists of three
45 steps with the described composition. Before starting the digestion process, nanomaterials
46 were freshly dispersed via ultrasonication in saliva and 0.05% BSA before addition of
47 digestion enzymes. As a control, ionic aluminum (AlCl_3) was used in the same concentration
48 ranges and treated accordingly. Then, 28 mL of synthetic saliva with the corresponding
49 samples were heated to 37 °C in a water bath and stirred for 5 min. Subsequently, a 10 mL
50 sample was taken for further analysis, 42 mL of artificial gastric juice were added to the
51 solution, and the pH value was set to 2 using hydrochloric acid. The solution was stirred for 2
52 h at 37 °C and the pH value was monitored every 30 min. Prior to the intestinal step, a 10 mL
53 sample was taken for further analysis. Then, 50 mL of artificial intestinal juice were added,
54
55
56
57
58
59
60

1
2
3 the pH value was set to 7.5 by adding sodium bicarbonate powder to the reaction solution,
4 and the solution was stirred for 2 more hours. Subsequently, intestinal samples were taken
5 for further analysis.
6

7
8 The activity of the digestion enzymes was verified prior to every set of experiments using
9 distinct control substrates for each step of the digestion process. Amylase activity was
10 confirmed using amylopectin azure, pepsin activity by using an albumin/bromophenol blue
11 complex, tryptic activity by using azocasein, and lipase activity by using 4-methylumbelliferyl
12 oleate as substrates, respectively. All resulting cleavage products were photometrically
13 monitored. In that way we could prove that all enzymes remained functional during the
14 experimental steps.
15
16
17
18
19
20

21 Transmission Electron Microscopy (TEM)

22
23 A drop of each digested or undigested sample was placed on a formvar carbon-coated 300
24 mesh grid for 20s for adsorption. Excess fluid was wicked off using a filter paper before grids
25 were air-dried. All grids were examined with a JEOL 1400 transmission electron microscope
26 (JEOL, Peabody MA, USA) operated at 120 kV and supplied with a GATAN Orius 1000
27 camera (GATAN Inc., Pleasanton CA, USA).
28
29
30
31
32

33 Small-angle X-ray scattering (SAXS)

34
35 SAXS measurements were conducted in a flow-through capillary with a Kratky-type
36 instrument (SAXSess from Anton Paar AG, Graz, Austria) at 21 ± 1 °C. The SAXSess has a
37 low sample-detector-distance of 0.309 m which is appropriate for the investigation of
38 dispersions with low scattering intensities. The experiments were performed with 120
39 measurement cycles (each averaged over 10 s). The measurements were background-
40 corrected with the respective mixture of aqueous BSA solution or digestive juices without
41 addition of aluminum species. Deconvolution (slit length desmearing) of the SAXS curves
42 was performed with the SAXS-Quant software (Anton Paar AG). Samples analyzed with
43 SAXS were used as prepared. Curve fitting was performed with the software McSAS (Monte
44 Carlo method, version 1.0.1). This procedure was described before ²⁷.
45
46
47
48
49
50
51
52

53 Single-particle inductively coupled plasma mass spectrometry (SP-ICP-MS)

54
55 For single particle analysis of the nanoparticle solutions a quadrupole ICP-MS (Thermo
56 Scientific iCAP Q, Thermo Fisher Scientific GmbH, Dreieich, Germany) with a PFA ST
57 Nebulizer, a quartz cyclonic spray chamber and a 2.5 mm quartz O-ring-free injector (all from
58
59
60

1
2
3 ESI Elemental Service & Instruments GmbH, Mainz, Germany) was used. Using the time-
4 resolved analysis mode for data acquisition intensities as a function of time (counts per
5 dwell-time interval) were collected. The acquisition time for each run was set to 60 s with a
6 dwell time (or data acquisition rate) of 3 ms. The gas flow for the plasma, the nebulizer and
7 the auxiliary (all Ar) were set to 13 L/min, 0.89 L/min and 0.7 L/min. The flow rate of the
8 sample was 0.34 mL/min. Data were exported to a spreadsheet developed by RIKILT
9 (Imperial Quality Control of Agricultural and Horticultural Products for further processing,
10 University of Wageningen, Netherlands). For data processing an established procedure
11 according to Pace *et al.*²⁸ was followed. Determination of nebulizer efficiency was performed
12 according to the described method with reference nanoparticles of known particle size. 60
13 nm gold reference nanoparticles from the U.S. National Institute of Standards and
14 Technology (NIST, RM 8013) were used as reference nanoparticles.
15
16
17
18
19
20
21
22
23

24 Ion beam microscopy (IBM)

25 IBM experiments were performed at LIPSION© nanoprobe. The singletron™ particle
26 accelerator was used to apply a 2.25 MeV proton beam according to a previously described
27 protocol²⁹. To avoid interactions between the ion beam and air molecules a vacuum with a
28 pressure of 5×10^{-5} and 10^{-7} Torr was applied. By focusing the beam, a spatial resolution of
29 around 1 μm was reached. For element analysis we used the X-ray fluorescence technique μ
30 proton-induced X-ray emission (μPIXE) and μ Rutherford Backscattering spectroscopy
31 (μRBS). Detection of μPIXE signals was done by a High Purity Germanium crystal detector
32 (Canberra, Meriden, CT, US). A 60 μm polyethylene layer was used to cover the detector for
33 backscattered protons. A Canberra PIPS-detector was used to detect the μRBS signal. For
34 element analysis the standard dispersion as well as gastric fluid was investigated. The
35 concentration of the nanoparticles in the digestion fluid was set to 1000 μg aluminum/ml.
36 Samples were prepared for measurements by centrifugation at 8,000 $\times g$ for 10 min.
37 Afterwards the supernatant was removed and replaced by mpH_2O followed by vortexing of
38 the sample. This procedure was repeated three times. Finally a small drop of the dispersion
39 was placed on polypropylene foil and the liquid was vaporized.
40
41
42
43
44
45
46
47
48
49
50

51 Time of flight secondary ion mass spectrometry (ToF-SIMS)

52 10 μl of digested samples were dropped on gold wafers and air-dried. Ion images and
53 spectra were acquired as described before³⁰ using a ToF-SIMS V instrument (ION-TOF
54 GmbH, Münster, Germany) with a 30 keV nano-bismuth primary ion beam source ($[\text{Bi}]_x^{(y+)}$ -
55 cluster ion source with a BiMn emitter). The ion currents were 0.5 pA at 5 kHz using a
56 Faraday cup. A pulse of 0.7 ns from the bunching system resulted in a mass resolution that
57
58
59
60

usually exceeded 9000 (full width at half-maximum) at $m/z < 500$ in positive ion mode. The primary ion dose was controlled below 10^{12} ions cm^{-2} to ensure static SIMS conditions. Charge compensation on the sample was obtained by a pulsed electron flood gun with 20 eV electrons.

The primary ion gun scanned a field of view of $80 \mu\text{m} \times 80 \mu\text{m}$ applying a 512×512 pixel measurement raster. Once the primary ion gun was aligned, a ToF-SIMS mass spectrum was generated by summing the detected secondary ion intensities and plotting them against the mass channels. The data were evaluated using the Surface Lab software (ION-TOF GmbH, Münster, Germany).

Ion release measurements

Ion release of nanoparticles in stock dispersions and digestion fluids was determined by ultracentrifugation ($100,000 \times g$ for 1h at 4°C) followed by acidic hydrolysis of the supernatant (69% HNO_3 , 180°C for 20 min in an MLS-ETHOS Microwave system) and element analysis was conducted using a quadrupole ICP-MS (Thermo Scientific iCAP Q, Thermo Fisher Scientific GmbH) comparable to previous studies³¹. LOD and LOQ for Al were determined as 0.6 respectively 1.8 ppB. Results are given as percentile of the initially used aluminum amount.

Results and Discussion

Aluminum is one of the most abundant metals on earth, occurs in our food and is therefore also taken up orally. The chemical identity of aluminum is an important factor for its bioavailability and toxicological potential^{3, 32}. Therefore, this study focused on the behavior of different aluminum species during the digestion process after oral uptake. Three different aluminum species were used, which represent elementary metallic aluminum, mineral oxidized aluminum, and completely dissolved ionic aluminum. These three representative substances vary strongly in their physicochemical properties including reactivity, solubility and bioavailability^{2, 33} and therefore were analyzed stepwise throughout the digestion procedure (before digestion, in saliva, stomach fluid, and intestinal fluid). Each step is characterized by typical compositions of buffer, salts, protein components and pH values. Differences in ionic content, particle size, shape, element attachment, agglomeration and stability were analyzed using complementary techniques: Element analysis, SAXS, TEM, SP-ICP-MS, ToF-SIMS and IBM.

Shape of the nanoparticles

1
2
3 TEM analysis of undigested nanoparticles in Figure 2 shows polydisperse spherical particles
4 with diameters between 10 and 100 nm with prominent finger-like grow outs for Al^0 and
5 needle-like nanoparticles with about 5 x 30 nm size in loosely packed agglomerates for
6 Al_2O_3 , whereas no particles were detectable in AlCl_3 solution. During the digestion process
7 both nanoparticle species appeared to agglomerate and to be surrounded by organic
8 material, while their size range has not substantially changed. However, it has to be kept in
9 mind that preparation for TEM analysis may cause agglomeration due to the necessary
10 drying step. In the intestinal fluids, deagglomeration was observed. For aluminum ions,
11 nanoparticle-like structures with different densities were observed in intestinal fluid that were
12 not detectable in undigested samples, saliva, or gastric fluid.
13
14
15
16
17
18
19

20 Size distribution and agglomeration of the nanoparticles

21
22 SAXS results are shown in Figure 3 and Supplementary Figure 1. Both nanoparticle species
23 displayed different agglomeration characteristics in undigested dispersion. Elementary Al^0
24 nanoparticles display a broad size distribution with primary particle radii ≥ 8 nm. In contrast
25 Al_2O_3 nanoparticles show a more narrow size distribution of primary particles with core radii
26 between 5 and 10 nm (Figure 3B,C). Populations with higher radii resulted from
27 agglomerates and aggregates of these primary particles, as proven by TEM (Figure 2) and
28 represented either aluminum nanoparticles or Al_2O_3 -nanoparticles depending on the
29 nanoparticle species used, as proven by ToF-SIMS (see Figure 6). Aluminum ions formed no
30 detectable particles in undigested stocks. In comparison to the undigested dispersions, the
31 SAXS core radii for both aluminum species are not notably changing by the transfer in saliva
32 (Figure 3E,F). Also, no nanoparticles were detected for ionic aluminum samples (Figure 3D).
33 In contrast to the saliva, the next steps of the digestion procedure strongly influence the
34 agglomeration behavior of the nanoparticles. Especially in gastric juice at low pH, SAXS
35 measurements showed an increased mean radius (Supplementary Figure 1). Moreover, this
36 effect was most prominent at the lowest concentration of Al_2O_3 nanoparticles. At the next
37 digestion step, the intestine, the pH value is shifted to 7.5. There, deagglomeration occurs
38 resulting in primary particles in the nano-scaled range. The core radii were now in the range
39 of the original state as found in the saliva. Surprisingly, the ionic aluminum samples also
40 showed detectable nano-scaled particles in the last step of the digestion process (Figure 3J)
41 which could be attributed to aluminum particles using ToF-SIMS analysis (see Figure 6G).
42
43
44
45
46
47
48
49
50
51
52

53 As a second method to determine size distributions, SP-ICP-MS measurements were
54 performed (Figure 4). Both particles species tended to stay unaffected in the saliva while in
55 the stomach only a small fraction of nanoparticles still remained in the nano-scaled range.
56 Especially for Al_2O_3 nanoparticles, the data indicate very high diameters that derive from
57
58
59
60

1
2
3 agglomeration in every artificial fluid. The lower limit of the SP-ICP-MS, based on the particle
4 mass, is directly dependent on the particle density, which leads to a particle-specific cutoff
5 diameter. In digested Al_2O_3 samples, there were no primary particles visible up to 200 nm.,
6 This may be due to non-spherical particles and the resulting agglomerates, which was
7 confirmed by TEM measurements (Figure 2). As a second reason, this can be resulting from
8 the complex medium that aggravates the mathematical calculation formula. Up to now,
9 based on the used mathematical algorithm for SP-ICP-MS, reliable size determination is
10 limited to spherical entities. Given the analytical background of aluminum as a consequence
11 of the ubiquitous presence of this element, the limit of detection is higher as compared to
12 rare elements e.g. gold. On the other hand, *de novo*-emerged nanoscaled particles formed
13 from AlCl_3 could not be proven by this method. Some signals were present in the time scan
14 which, however, did not lead to calculable size distributions.
15
16
17
18
19
20
21
22
23

24 Ion release of the nanoparticles

25 The free ionic fraction of aluminum was separated by centrifugation from the particulate and
26 matrix-bound aluminum fraction and analyzed via ICP-MS after acidic hydrolysis (Figure 5).
27 As shown in Figure 5B,C, both particle species displayed a very low intrinsic ion release
28 below 0.03% in undigested dispersion. Similar values were obtained for the ionic content in
29 saliva (Figure 5E,F). In gastric media (Figure 5H,I), metallic Al^0 nanoparticles released with a
30 value of 3 % slightly more ions while Al_2O_3 nanoparticles appear to be more inert in terms of
31 solubility. In intestinal fluid, free ions disappeared almost completely. Ion controls showed
32 almost 100% free ions in stocks, saliva and gastric fluid (Figure 5A, D, G), while there was a
33 severe decrease of free ions in the intestinal fluid (Figure 5J). This matches well to the TEM
34 data and SAXS spectra showing particle formation from dissolved aluminum (Figure 2,
35 Figure 3).
36
37
38
39
40
41
42
43
44

45 Element distribution of aluminum - Time of flight secondary ion mass spectrometry (TOF- 46 SIMS)

47 ToF-SIMS results are shown in Figure 6. No pronounced agglomeration was found in saliva
48 samples (Figure 6B, C), whereas we determined strong agglomeration spots in the stomach
49 fluid, as indicated by colored circles (Figure 6E, F). For Al_2O_3 nanoparticles, these intense
50 spots disappeared in the intestine, while there were strong agglomerated spots still present
51 for the metallic Al^0 nanoparticles (Figure 6H, I). We could not detect aluminum-containing
52 spots in the AlCl_3 samples in saliva and stomach fluid, while there were some measurable
53 accumulation spots of aluminum in the intestine fluid which, however, appeared much
54 weaker than in the nanoparticle samples (Figure 6G).
55
56
57
58
59
60

Elements associated to aluminum

IBM measurements were used for the analysis of elements associated with the aluminum nanoparticles (Figure 7). We investigated undigested nanoparticle samples as well as digested particles and ionic samples in the intestinal fluid after artificial digestion μ PIXE images visualize the location of Al particles and co-localization P, K and Ca elements with Al (Figure 7). The amount of co-localized elements for particles prepared following the artificial digestion were analyzed. The concentration of sulfur on the NP surface was the same for undigested Al and Al_2O_3 particles. This finding reflects the presence of the same amount of albumin corona build on the surface of particles after standard treatment. After digestion the amount of sulfur decreased by a quotient larger ten for both particles. It could be concluded that the albumin corona was removed to a large extent during digestion process. The reason could be the change of pH value during digestion treatment. This leads to the recharging of albumin having an isoelectrical point at a value of 4.6. Partially removing of the protein corona might be the result of this treatment. De novo emerged particles deriving from AlCl_3 appear to have a higher sulfur amount than both other species. Precipitation with proteins, such as mucin or trypsin from the artificial media, or attachment of sulfide ions might describe this behavior. The digested Al and Al_2O_3 as well as *de novo* Al particles reveal the same level of P and Ca elements, The concentration of these elements increased by a two order of magnitude in case of Al_2O_3 particles. The high amount of these elements for digested particles might result from attachment of calcium and phosphate ions, which build a calcium phosphate layer on particle surface. Chlorine and Potassium increased more in the metallic Al particle samples than in the Al_2O_3 samples. Only a small amount of iron and zinc, deriving from the digestion fluids, is associated to aluminum after the digestion process.

Discussion

Protein composition in artificial saliva is slightly more complex than BSA used in standard dispersion, but does not contain proteins or salts that are expected to provoke the formation of completely new chemical entities or complexes with altered chemical characteristics. As a result, in artificial saliva the properties of the nanomaterials do not differ strongly from those of the undigested samples. In our experiments, artificial saliva did not lead to aggregation or dissolution of neither Al^0 , nor Al_2O_3 nanoparticles. Also the formation of new particle populations resulting from free ions was not observed for all Al species.

Stomach fluid is characterized by higher ionic strength and a more acidic environment with a pH value in the range of 2²². Previous studies detected a general tendency of nanoparticles to aggregate at low pH values due to the electrostatic destabilization, for example silver^{19, 21}

1
2
3 or silica^{25, 34} or show enhanced ion release in the gastric fluid in case of silver^{20-21, 35} and
4 zinc oxide³⁴. In this study, we were able to prove that these effects are also observable for
5 Al-containing nanoparticles. We found agglomeration in TEM, ToF-SIMS and SAXS
6 combined with a disappearance of nano-scaled particles in SP-ICP-MS. We also detected
7 ion release from both particle species in gastric fluid, but to a very low extent, thus excluding
8 predominant dissolution of the particles. We suggest that a small amount of ions goes into
9 solution without remarkably changing the mean radii of the primary particles. As expected, a
10 slightly higher ion release occurs from the metallic than from the mineral form of Al. Free Al
11 ions can bind to or build complexes with proteins and biological compounds contained in
12 foods, as well as with biological structures of the intestinal tissue^{3, 36-37}. Recent studies
13 showed that this is not necessarily connected to an increased toxicity *in vitro*²¹, but that the
14 phenomenon can lead to increased cellular particle uptake depending on the composition of
15 the digestive juices and therein-contained food components²⁰.

16
17
18
19
20
21
22
23 The most remarkable physico-chemical changes occurred at the transition from the artificial
24 stomach fluid to the intestinal fluid, which simulates the passage into the duodenum. There,
25 pH increases to 7.5 and bile extract is added. TEM, SAXS, SP-ICP-MS and ToF-SIMS
26 showed a reconstitution of the state and particle size measured before in saliva fluid. This
27 means that all observed Al species, including soluble AlCl₃, reach the intestine partly as
28 nanoparticles. ICP-MS showed a decrease of free ions in digested samples for both primary
29 particle species (metallic and mineral oxidized Al), suggesting the formation of complexes or
30 aggregates. Furthermore, a strong decrease of free ions in the AlCl₃ solution was detected
31 as well concomitantly to the presence of nano-scaled structures in the intestinal fluid. ToF-
32 SIMS and μ PIXE images also showed agglomerates deriving from AlCl₃ samples that were
33 not detected previously, neither in saliva nor in gastric fluid. TEM-pictures show newly
34 emerging nanoscaled, particle-like structures that differ in shape and density from the other
35 applied primary particles. ToF-SIMS proved that these aggregates contain aluminum and
36 IBM revealed the co-localization of aluminum with sulfur elements. The presence of sulfur
37 detected in *de novo* particles supports the assumption about formation of precipitated Al-
38 protein nanocomplexes. Furthermore, calcium phosphate layer was found on particle surface
39 for all three aluminum species. The formation of this layer could impact significantly on the
40 cellular uptake and the bioavailability of nanoparticles.³⁸⁻³⁹

41
42
43
44
45
46
47
48
49
50
51 In conclusion we postulate these structures to be metal-organic particle-like complexes that
52 are predominantly in the nano-scaled range. This difference in density and chemical
53 composition, as compared to the Al⁰ and Al₂O₃ particles also used in the study, is the
54 suspected reason why they cannot be detected in SP-ICP-MS.

55
56
57
58
59
60
With the help of SAXS we observed a particle size distribution with a volume-weighted mean
radius of 2.9 nm for the particle population formed *de novo*. The issue of *de novo* formation

1
2
3 of particles as part of a transition between particulate and ionic species has, up to now, not
4 been in the primary focus of research. Comparable *de novo* particle formation, as well as
5 nanoparticles overcoming the digestion process, has also been observed for silver⁴⁰⁻⁴¹.
6 Although soluble compounds precipitate or agglomerate due to changing physico-chemical
7 conditions, it is noteworthy that a significant amount of these *de novo*-emerged particles are
8 in the nano-scaled range. Therefore they might have nano-specific characteristics, including
9 enhanced reactivity and altered uptake. Furthermore, when talking about toxicological
10 analyses of nanomaterials one should keep in mind that there is a certain balance between
11 dissolved, agglomerated and non-agglomerated nanoparticulate species deriving from the
12 same origin. These conversion processes occur bi-directionally and differ significantly among
13 the multiple biological environments. Up to now, little is known about the two-directional
14 solubilization behavior of metallic nanoparticles. We observed a severe change of the
15 chemical state of dissolved aluminum between stomach and small intestine. Figure 8
16 summarizes possible transitions between free ions, nanoparticles and agglomerates during
17 the digestion process. Experimental evidence for the scenario drafted in Figure 8 has also
18 been depicted in this study for aluminum and was observed in previous studies for silver^{20-21,}
19 ³⁵. Even if *de novo* formation of nano-scaled particles from other metals like Silver has not
20 been experimentally shown in intestinal fluid, physicochemical similarities of different metals,
21 as well as shared affinity to biological structures, suggest that *de novo* formation of
22 nanoparticles might also occur from additional metals following oral uptake of dissolved ions.
23
24
25
26
27
28
29
30
31
32
33

34 Altogether, we used a broad spectrum of methods to characterize the behavior of different
35 aluminum species during an *in vitro* digestion process. As no single method is capable of
36 depicting the different modifications, it is necessary to use complementary analytical
37 techniques for a systematic characterization of physicochemical properties of nanomaterials.
38 Such strategy will bring comprehensive knowledge to investigate nanomaterials and their
39 fate in relevant biological media and to link these results with the toxicological potential. For
40 this purpose, it is indispensable to take into account the different transitions leading to a
41 mixture of ionic, particulate and agglomerated species from one pristine material.
42
43
44
45
46
47

48 **Summary and Conclusions**

49 During the digestion process, metallic and oxidized aluminum particles undergo physico-
50 chemical conversions depending on their biological environment. While staying almost
51 unaffected in saliva, they preferably agglomerate in gastric juice and, also slightly release
52 ions into the fluid. After transition into intestine the agglomerates tend to de-agglomerate into
53 primary particles again, whereas free ions form solid complexes with biological compounds.
54 These complexes can be nano-scaled and differ significantly from primary particles in their
55 size, shape and density. Particles and dissolved ions can be transformed into each other and
56
57
58
59
60

1
2
3 their surface element composition can change. A broad spectrum of methods is required to
4 characterize all these parameters adequately. With respect to this knowledge, toxicological
5 investigations of individual nanoparticle species are only purposeful with regard to the
6 respective biological and chemical environment. By demonstrating the mutual conversion of
7 nano-particles and dissolved metal ions, the present data underline that it might not be
8 possible to distinguish between particle- and ion-dependent effects in toxicological studies.
9 Careful physicochemical characterization will be essential for proper interpretation of toxicity
10 data.
11
12
13
14
15

16 Declaration of interest

17 The authors declare no conflict of interest.
18
19
20
21

22 Acknowledgements

23 This publication, as part of the German-French SolNanoTOX project was funded by the
24 German Research Foundation DFG (Grant Numbers LA 3411/1-1), by the French "Agence
25 Nationale de la Recherche" ANR (Project ID ANR-13-IS10-0005).
26
27
28
29
30
31

32 References

- 33
34 1. Willhite, C. C.; Ball, G. L.; McLellan, C. J., Total allowable concentrations of monomeric
35 inorganic aluminum and hydrated aluminum silicates in drinking water. *Critical reviews in*
36 *toxicology* **2012**, *42* (5), 358-442.
37 2. Yokel, R. A.; Florence, R. L., Aluminum bioavailability from the approved food additive
38 leavening agent acidic sodium aluminum phosphate, incorporated into a baked good, is
39 lower than from water. *Toxicology* **2006**, *227* (1-2), 86-93.
40 3. Yokel, R. A.; McNamara, P. J., Aluminium toxicokinetics: an updated minireview.
41 *Pharmacology & toxicology* **2001**, *88* (4), 159-67.
42 4. Lote, C. J.; Saunders, H., Aluminium: gastrointestinal absorption and renal excretion.
43 *Clinical science (London, England : 1979)* **1991**, *81* (3), 289-95.
44 5. Exley, C., The toxicity of aluminium in humans. *Morphologie* **2016**, *100* (329), 51-5.
45 6. Wagner, W., *Canadian Minerals Yearbook. Ottawa: Natural Resources Canada*. 1999.
46 7. Savory, J.; Bertholf, R. L.; Wills, M. R., Aluminium toxicity in chronic renal insufficiency.
47 *Clinics in endocrinology and metabolism* **1985**, *14* (3), 681-702.
48 8. Walton, J. R., Chronic aluminum intake causes Alzheimer's disease: applying Sir Austin
49 Bradford Hill's causality criteria. *J Alzheimers Dis* **2014**, *40* (4), 765-838.
50 9. Darbre, P. D., Underarm antiperspirants/deodorants and breast cancer. *Breast Cancer*
51 *Res* **2009**, *11 Suppl 3*, S5.
52 10. Greger, J. L., Dietary and other sources of aluminium intake. *Ciba Foundation*
53 *symposium* **1992**, *169*, 26-35; discussion 35-49.
54 11. Yang, Y.; Doudrick, K.; Bi, X.; Hristovski, K.; Herckes, P.; Westerhoff, P.; Kaegi, R.,
55 Characterization of food-grade titanium dioxide: the presence of nanosized particles.
56 *Environ Sci Technol* **2014**, *48* (11), 6391-400.
57 12. Faust, J. J.; Doudrick, K.; Yang, Y.; Capco, D. G.; Westerhoff, P., A Facile Method for
58 Separating and Enriching Nano and Submicron Particles from Titanium Dioxide Found in
59 Food and Pharmaceutical Products. *PLoS One* **2016**, *11* (10), e0164712.
60

13. Golja, V.; Drazic, G.; Lorenzetti, M.; Vidmar, J.; Scancar, J.; Zalaznik, M.; Kalin, M.; Novak, S., Characterisation of food contact non-stick coatings containing TiO₂ nanoparticles and study of their possible release into food. *Food Addit Contam Part A Chem Anal Control Expo Risk Assess* **2016**.
14. Echegoyen, Y.; Nerin, C., Nanoparticle release from nano-silver antimicrobial food containers. *Food Chem Toxicol* **2013**, *62*, 16-22.
15. Lin, Q. B.; Li, H.; Zhong, H. N.; Zhao, Q.; Xiao, D. H.; Wang, Z. W., Migration of Ti from nano-TiO₂-polyethylene composite packaging into food simulants. *Food Addit Contam Part A Chem Anal Control Expo Risk Assess* **2014**, *31* (7), 1284-90.
16. Nel, A.; Xia, T.; Madler, L.; Li, N., Toxic potential of materials at the nanolevel. *Science (New York, N.Y.)* **2006**, *311* (5761), 622-7.
17. Di Silvio, D.; Rigby, N.; Bajka, B.; Mackie, A.; Baldelli Bombelli, F., Effect of protein corona magnetite nanoparticles derived from bread in vitro digestion on Caco-2 cells morphology and uptake. *The international journal of biochemistry & cell biology* **2016**, *75*, 212-22.
18. Oomen, A. G.; Hack, A.; Minekus, M.; Zeijdner, E.; Cornelis, C.; Schoeters, G.; Verstraete, W.; Van de Wiele, T.; Wragg, J.; Rompelberg, C. J.; Sips, A. J.; Van Wijnen, J. H., Comparison of five in vitro digestion models to study the bioaccessibility of soil contaminants. *Environ Sci Technol* **2002**, *36* (15), 3326-34.
19. Walczak, A. P.; Fokkink, R.; Peters, R.; Tromp, P.; Herrera Rivera, Z. E.; Rietjens, I. M.; Hendriksen, P. J.; Bouwmeester, H., Behaviour of silver nanoparticles and silver ions in an in vitro human gastrointestinal digestion model. *Nanotoxicology* **2013**, *7* (7), 1198-210.
20. Lichtenstein, D.; Ebmeyer, J.; Knappe, P.; Juling, S.; Bohmert, L.; Selve, S.; Niemann, B.; Braeuning, A.; Thunemann, A. F.; Lampen, A., Impact of food components during in vitro digestion of silver nanoparticles on cellular uptake and cytotoxicity in intestinal cells. *Biol Chem* **2015**, *396* (11), 1255-64.
21. Böhmert, L.; Girod, M.; Hansen, U.; Maul, R.; Knappe, P.; Niemann, B.; Weidner, S. M.; Thunemann, A. F.; Lampen, A., Analytically monitored digestion of silver nanoparticles and their toxicity on human intestinal cells. *Nanotoxicology* **2014**, *8* (6), 631-42.
22. Versantvoort, C. H.; Oomen, A. G.; Van de Kamp, E.; Rompelberg, C. J.; Sips, A. J., Applicability of an in vitro digestion model in assessing the bioaccessibility of mycotoxins from food. *Food Chem Toxicol* **2005**, *43* (1), 31-40.
23. Gerloff, K.; Pereira, D. I.; Faria, N.; Boots, A. W.; Kolling, J.; Forster, I.; Albrecht, C.; Powell, J. J.; Schins, R. P., Influence of simulated gastrointestinal conditions on particle-induced cytotoxicity and interleukin-8 regulation in differentiated and undifferentiated Caco-2 cells. *Nanotoxicology* **2013**, *7* (4), 353-66.
24. Kästner, C.; Lichtenstein, D.; Lampen, A.; Thunemann, A. F., Monitoring the fate of small silver nanoparticles during artificial digestion. *Colloids and Surfaces A: Physicochemical and Engineering Aspects* **2016**.
25. Peters, R.; Kramer, E.; Oomen, A. G.; Rivera, Z. E.; Oegema, G.; Tromp, P. C.; Fokkink, R.; Rietveld, A.; Marvin, H. J.; Weigel, S.; Peijnenburg, A. A.; Bouwmeester, H., Presence of nano-sized silica during in vitro digestion of foods containing silica as a food additive. *ACS Nano* **2012**, *6* (3), 2441-51.
26. Hur, S. J.; Lee, S. Y.; Lee, S. J., Effect of biopolymer encapsulation on the digestibility of lipid and cholesterol oxidation products in beef during in vitro human digestion. *Food Chem* **2015**, *166*, 254-60.
27. Kastner, C.; Thunemann, A. F., Catalytic Reduction of 4-Nitrophenol Using Silver Nanoparticles with Adjustable Activity. *Langmuir* **2016**, *32* (29), 7383-91.
28. Pace, H. E.; Rogers, N. J.; Jarolimek, C.; Coleman, V. A.; Higgins, C. P.; Ranville, J. F., Determining transport efficiency for the purpose of counting and sizing nanoparticles via single particle inductively coupled plasma mass spectrometry. *Analytical chemistry* **2011**, *83* (24), 9361-9.
29. Lichtenstein, D.; Ebmeyer, J.; Meyer, T.; Behr, A. C.; Kastner, C.; Böhmert, L.; Juling, S.; Niemann, B.; Fahrenson, C.; Selve, S.; Thunemann, A. F.; Meijer, J.; Estrela-Lopis, I.; Braeuning, A.; Lampen, A., It takes more than a coating to get nanoparticles through the

- 1
2
3 intestinal barrier in vitro. *European journal of pharmaceutics and biopharmaceutics : official journal of Arbeitsgemeinschaft fur Pharmazeutische Verfahrenstechnik e.V* **2016**.
- 4
5 30. Jungnickel, H.; Pund, R.; Tentschert, J.; Reichardt, P.; Laux, P.; Harbach, H.; Luch, A.,
6 Time-of-flight secondary ion mass spectrometry (ToF-SIMS)-based analysis and imaging
7 of polyethylene microplastics formation during sea surf simulation. *The Science of the*
8 *total environment* **2016**, 563-564, 261-6.
- 9 31. Hsiao, I. L.; Bierkandt, F. S.; Reichardt, P.; Luch, A.; Huang, Y. J.; Jakubowski, N.;
10 Tentschert, J.; Haase, A., Quantification and visualization of cellular uptake of TiO₂ and
11 Ag nanoparticles: comparison of different ICP-MS techniques. *Journal of*
12 *nanobiotechnology* **2016**, 14 (1), 50.
- 13 32. Willhite, C. C.; Karyakina, N. A.; Yokel, R. A.; Yenugadhati, N.; Wisniewski, T. M.;
14 Arnold, I. M.; Momoli, F.; Krewski, D., Systematic review of potential health risks posed
15 by pharmaceutical, occupational and consumer exposures to metallic and nanoscale
16 aluminum, aluminum oxides, aluminum hydroxide and its soluble salts. *Critical reviews in*
17 *toxicology* **2014**, 44 Suppl 4, 1-80.
- 18 33. Exley, C., A biogeochemical cycle for aluminium? *Journal of inorganic biochemistry*
19 **2003**, 97 (1), 1-7.
- 20 34. McCracken, C.; Zane, A.; Knight, D. A.; Dutta, P. K.; Waldman, W. J., Minimal intestinal
21 epithelial cell toxicity in response to short- and long-term food-relevant inorganic
22 nanoparticle exposure. *Chemical research in toxicology* **2013**, 26 (10), 1514-25.
- 23 35. Liu, J.; Hurt, R. H., Ion release kinetics and particle persistence in aqueous nano-silver
24 colloids. *Environ Sci Technol* **2010**, 44 (6), 2169-75.
- 25 36. Murko, S.; Milacic, R.; Scancar, J., Speciation of Al in human serum by convective-
26 interaction media fast-monolithic chromatography with inductively coupled plasma mass
27 spectrometric detection. *Journal of inorganic biochemistry* **2007**, 101 (9), 1234-41.
- 28 37. Ruiperez, F.; Mujika, J. I.; Ugalde, J. M.; Exley, C.; Lopez, X., Pro-oxidant activity of
29 aluminum: promoting the Fenton reaction by reducing Fe(III) to Fe(II). *Journal of*
30 *inorganic biochemistry* **2012**, 117, 118-23.
- 31 38. Dordelmann, G.; Kozlova, D.; Karczewski, S.; Lizio, R.; Knauer, S.; Epple, M., Calcium
32 phosphate increases the encapsulation efficiency of hydrophilic drugs (proteins, nucleic
33 acids) into poly(D,L-lactide-co-glycolide acid) nanoparticles for intracellular delivery. *J*
34 *Mater Chem B* **2014**, 2 (41), 7250-7259.
- 35 39. Morgan, T. T.; Muddana, H. S.; Altinoglu, E. I.; Rouse, S. M.; Tabakovic, A.; Tabouillot,
36 T.; Russin, T. J.; Shanmugavelandy, S. S.; Butler, P. J.; Eklund, P. C.; Yun, J. K.; Kester,
37 M.; Adair, J. H., Encapsulation of Organic Molecules in Calcium Phosphate
38 Nanocomposite Particles for Intracellular Imaging and Drug Delivery. *Nano Lett* **2008**, 8
39 (12), 4108-4115.
- 40 40. Juling, S.; Bachler, G.; von Gotz, N.; Lichtenstein, D.; Bohmert, L.; Niedzwiecka, A.;
41 Selve, S.; Braeuning, A.; Lampen, A., In vivo distribution of nanosilver in the rat: The role
42 of ions and de novo-formed secondary particles. *Food Chem Toxicol* **2016**, 97, 327-335.
- 43 41. Hansen, U.; Thünemann, A. F., Characterization of Silver Nanoparticles in Cell Culture
44 Medium Containing Fetal Bovine Serum. *Langmuir* **2015**, 31 (24), 6842-52.
- 45
46
47
48

Figure legends

49
50
51
52 Figure 1: Scheme of particle dispersion and *in vitro* digestion including the composition of
53 digestion fluids, experimental workflow and nanoparticle concentrations.

54
55
56
57 Figure 2: Representative TEM pictures of aluminum-containing samples after standard
58 dispersion (A-C), in artificial saliva (D-F), gastric fluid (G-I), and intestinal fluid (J-L). The
59
60

1
2
3 sample concentration applied to the grid was 0.8 g/L. AlCl_3 -containing samples showed no
4 measurable particles in stock, saliva and gastric fluid. Representative images are depicted.
5
6
7

8
9 Figure 3: Volume-weighted size distributions derived by SAXS measurements of samples
10 containing $\text{Al}(0)$ nanoparticles, Al_2O_3 nanoparticles and AlCl_3 , respectively, after standard
11 dispersion (A-C), in artificial saliva (D-F), gastric fluid (G-I), and intestinal fluid (J-L). The
12 distributions of undigested stock solutions and digested Al^0 nanoparticles, Al_2O_3
13 nanoparticles, and AlCl_3 in their highest concentration are given (6.67 mg Al/mL at the
14 beginning of digestion process in saliva and 1 mg Al/mL at the end in intestinal fluid). AlCl_3 -
15 containing samples showed no measurable particles in stock solution, saliva and gastric
16 fluid. The right hand y-axes mark the cumulative particle fraction presentation given in blue
17 solid lines. The size distributions are fitted by a lognormal distribution function (red solid
18 lines).
19
20
21
22
23
24
25

26
27 Figure 4: Number-weighted size-distributions of aluminum samples after standard dispersion
28 (A-C), in artificial saliva (D-F), gastric fluid (G-I), and intestinal fluid (J-L). Representative
29 images and size distributions are calculated from 60 s measuring time each run. For
30 intestinal samples, the time scan is shown, too (M-O). The number of measurable particles in
31 AlCl_3 -containing samples was too low to calculate a size distribution.
32
33
34
35
36

37
38 Figure 5: Determination of free aluminum ions of aluminum-containing samples after
39 standard dispersion (A-C), in artificial saliva (D-F), gastric fluid (G-I), and intestinal fluid (J-L).
40 Quantification of ionic percentile determined by UC followed by nitric acid digestion and ICP-
41 MS is given. Each sample was performed twice and measured twice. Error bars show the
42 standard deviation of the mean values.
43
44
45

46
47 Figure 6: Representative ToF-SIMS images of aluminum-containing samples in artificial
48 saliva (A-C), gastric fluid (D-F), and intestinal fluid (G-I). AlCl_3 -containing samples showed no
49 measurable particles in saliva and gastric fluid. Densitograms show local agglomerations of
50 measured Al-species, indicated by colored circles.
51
52
53
54

55
56 Figure 7: Digestion impact on surface modification of nanoparticles. (A - F): Element analysis
57 of Al, of Al_2O_3 and *de novo* emerged particles resulted from AlCl_3 . Samples were prepared
58 following standard dispersion (A - C) as well as in intestinal fluid after having performed the
59
60

1
2
3 full artificial digestion protocol (D - F). Each sample was measured at least 3 times on
4 different positions. Error bars represent the standard deviation of the mean values. (G - I):
5 μ PIXE images of element distributions in Al species after artificial digestion process. All
6 images displaying an area of 25 x 25 μm^2 . The color code is as follow: minimal concentration
7 is displayed black, while maximum is shown as white.
8
9

10
11
12
13 Figure 8: Suggested scheme of aluminum particle dissolution and agglomeration during the
14 artificial digestion process. Samples stay unaffected in artificial saliva but agglomerate in the
15 stomach fluid. At the same time, ions are released from particles but incomplete dissolution
16 occurs. In intestinal fluid, agglomerates tend to de-agglomerate into primary particles and
17 free ions form nano-scaled particulate structures, too.
18
19
20
21
22
23
24
25
26
27
28
29
30
31
32
33
34
35
36
37
38
39
40
41
42
43
44
45
46
47
48
49
50
51
52
53
54
55
56
57
58
59
60

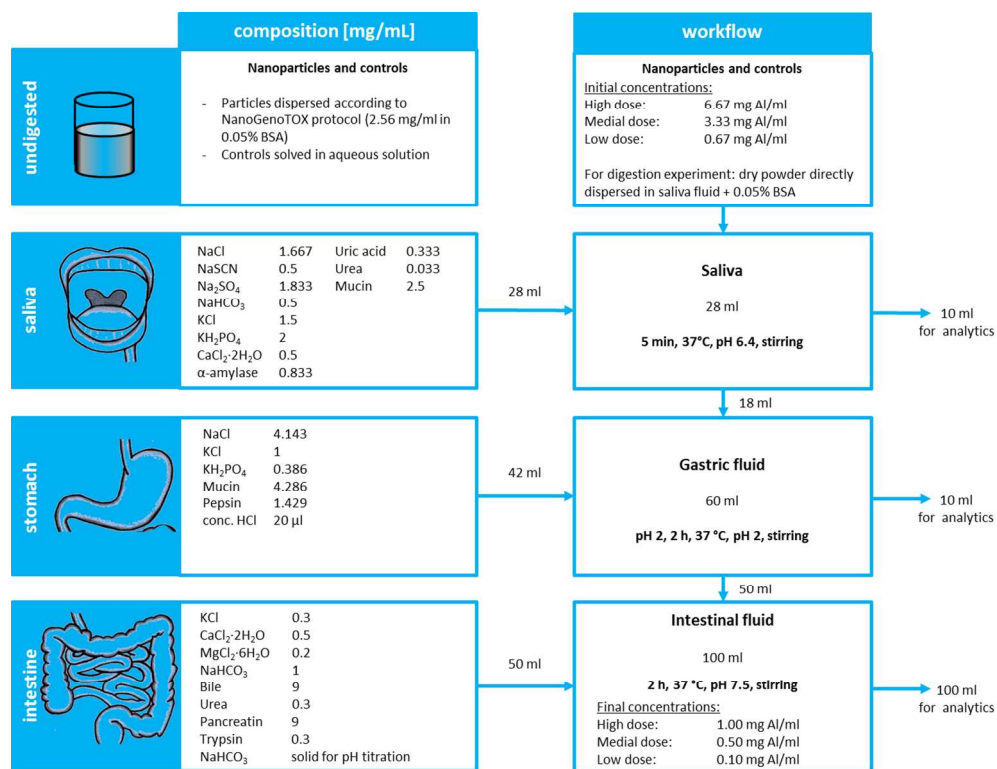


Figure 1: Scheme of particle dispersion and in vitro digestion including the composition of digestion fluids, experimental workflow and nanoparticle concentrations.

382x292mm (96 x 96 DPI)

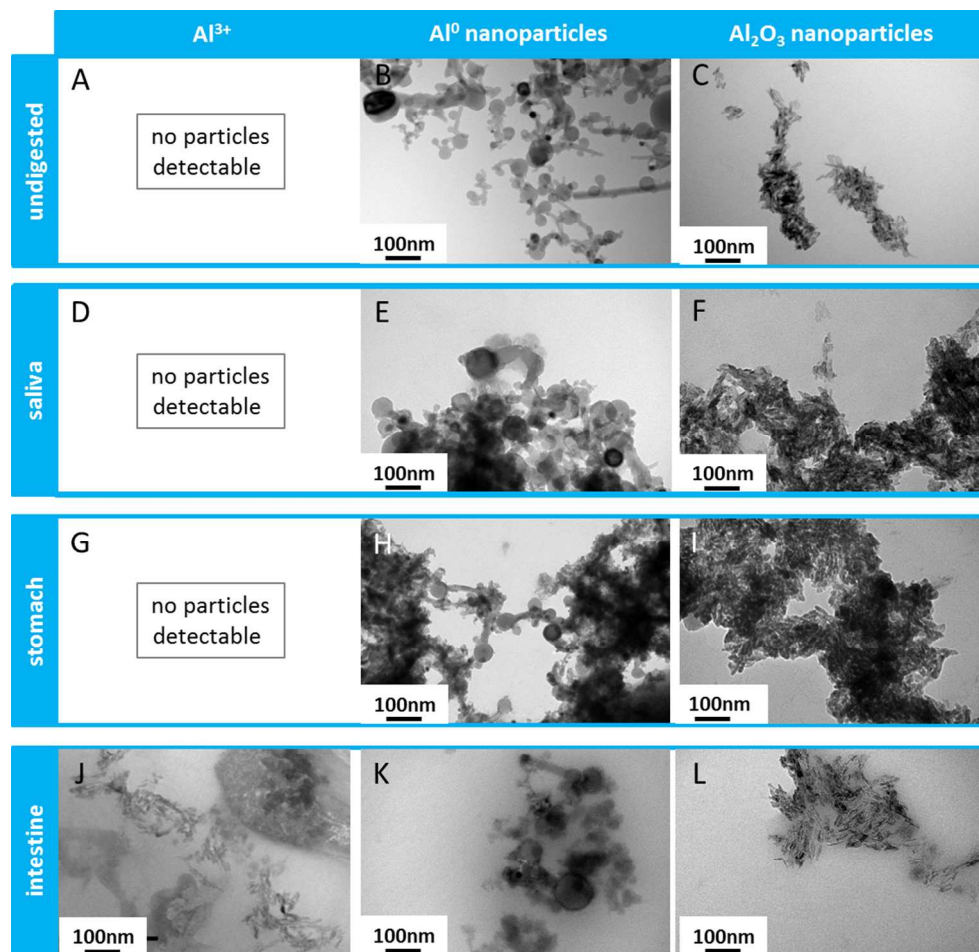


Figure 2: Representative TEM pictures of aluminum-containing samples after standard dispersion (A-C), in artificial saliva (D-F), gastric fluid (G-I), and intestinal fluid (J-L). The sample concentration applied to the grid was 0.8 g/L. $AlCl_3$ -containing samples showed no measurable particles in stock, saliva and gastric fluid. Representative images are depicted.

305x292mm (96 x 96 DPI)

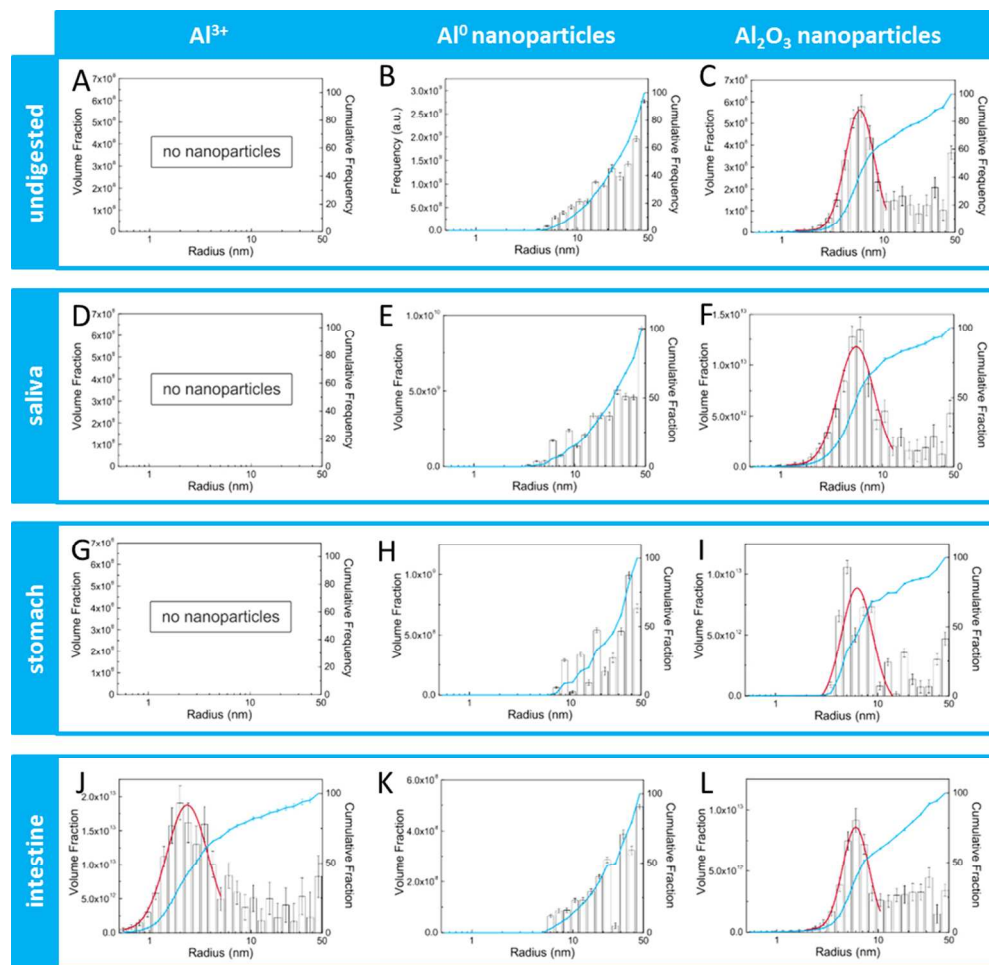


Figure 3: Volume-weighted size distributions derived by SAXS measurements of samples containing Al(0) nanoparticles, Al₂O₃ nanoparticles and AlCl₃, respectively, after standard dispersion (A-C), in artificial saliva (D-F), gastric fluid (G-I), and intestinal fluid (J-L). The distributions of undigested stock solutions and digested Al(0) nanoparticles, Al₂O₃ nanoparticles, and AlCl₃ in their highest concentration are given (6.67 mg Al/mL at the beginning of digestion process in saliva and 1 mg Al/mL at the end in intestinal fluid). AlCl₃-containing samples showed no measurable particles in stock solution, saliva and gastric fluid. The right hand y-axes mark the cumulative particle fraction presentation given in blue solid lines. The size distributions are fitted by a lognormal distribution function (red solid lines).

302x290mm (96 x 96 DPI)

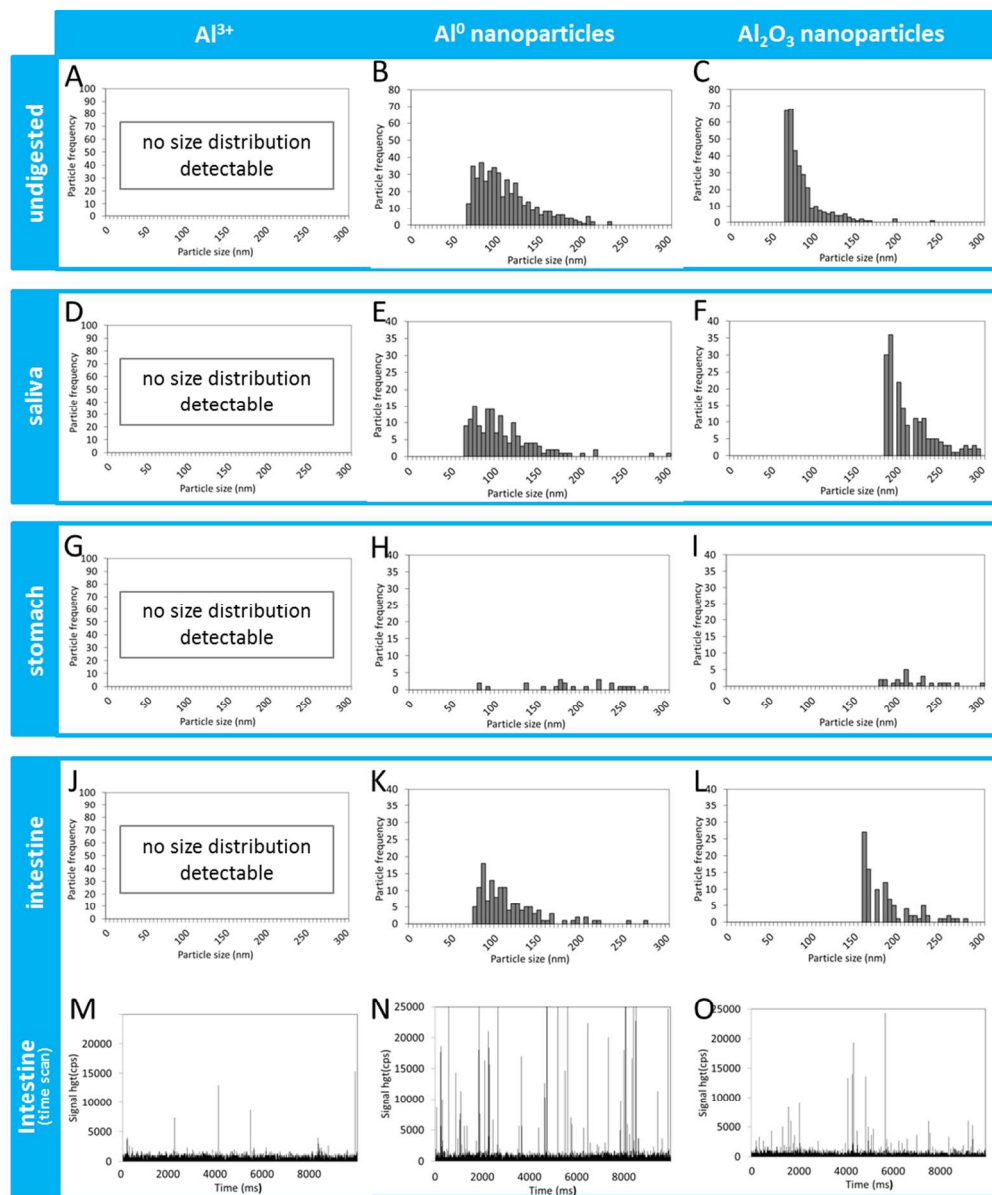


Figure 4: Number-weighted size-distributions of aluminum samples after standard dispersion (A-C), in artificial saliva (D-F), gastric fluid (G-I), and intestinal fluid (J-L). Representative images and size distributions are calculated from 60 s measuring time each run. For intestinal samples, the time scan is shown, too (M-O). The number of measurable particles in AlCl_3 -containing samples was too low to calculate a size distribution.

302x359mm (96 x 96 DPI)

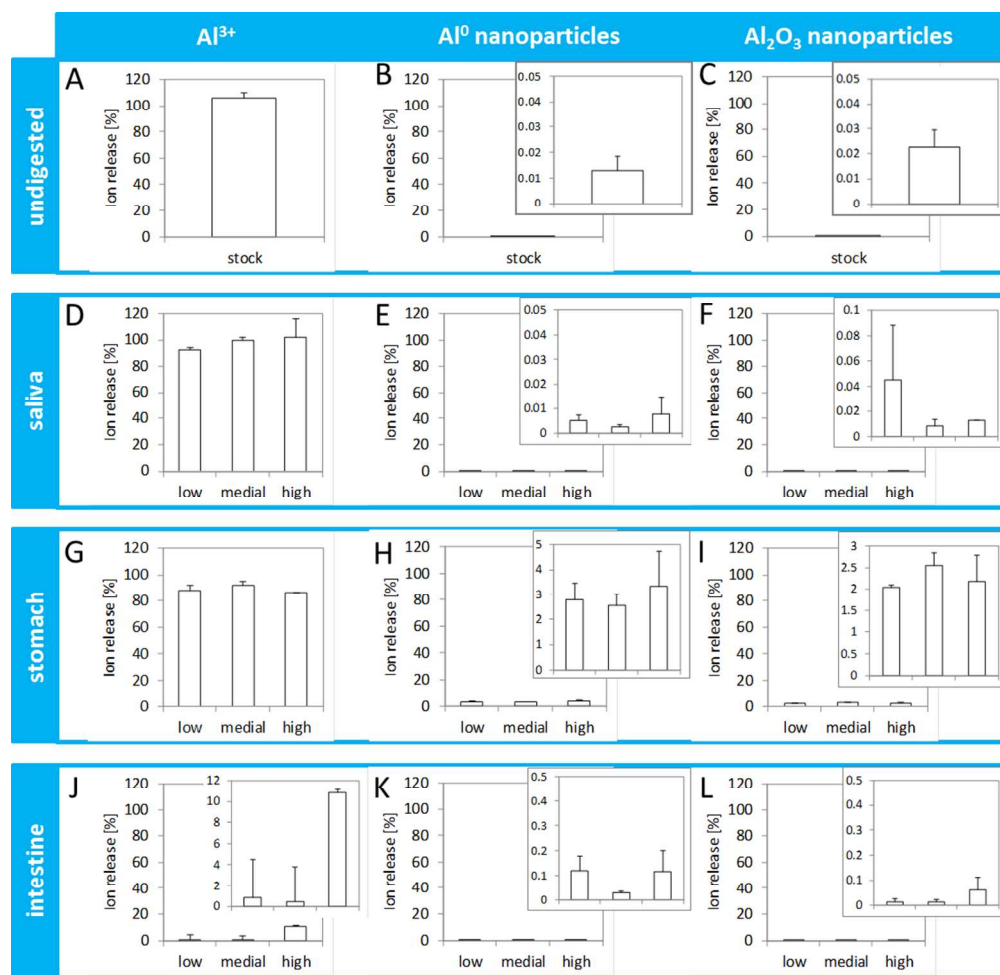


Figure 5: Determination of free aluminum ions of aluminum-containing samples after standard dispersion (A-C), in artificial saliva (D-F), gastric fluid (G-I), and intestinal fluid (J-L). Quantification of ionic percentile determined by UC followed by nitric acid digestion and ICP-MS is given. Each sample was performed twice and measured twice. Error bars show the standard deviation of the mean values.

299x290mm (96 x 96 DPI)

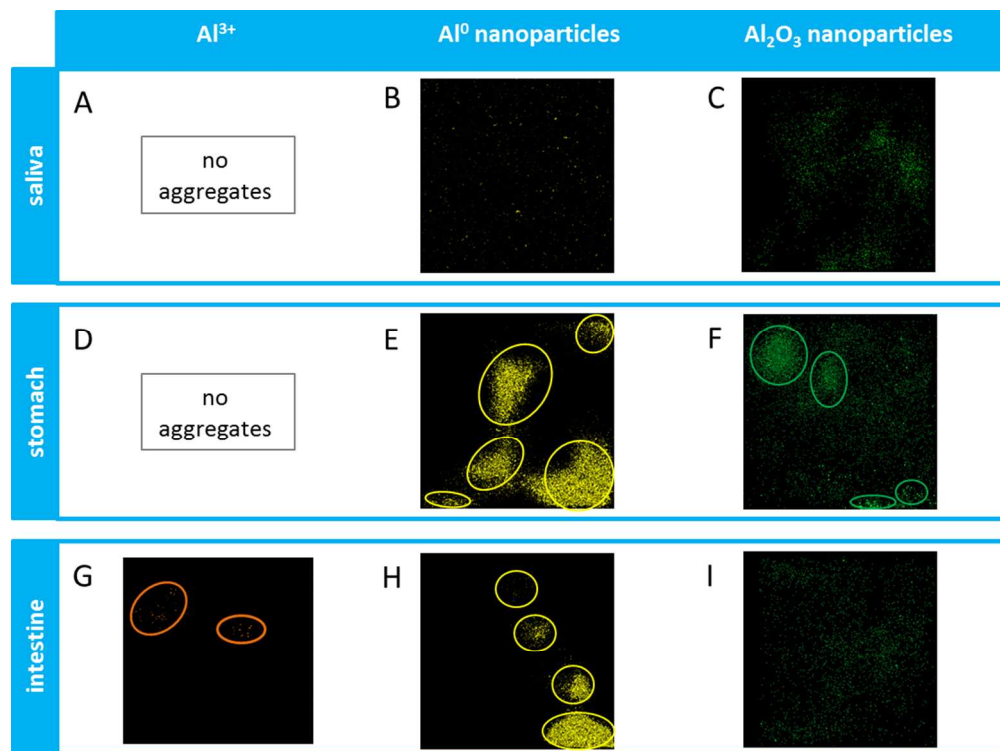


Figure 6: Representative ToF-SIMS images of aluminum-containing samples in artificial saliva (A-C), gastric fluid (D-F), and intestinal fluid (G-I). AlCl_3 -containing samples showed no measurable particles in saliva and gastric fluid. Densitograms show local agglomerations of measured Al-species, indicated by colored circles.

299x223mm (96 x 96 DPI)

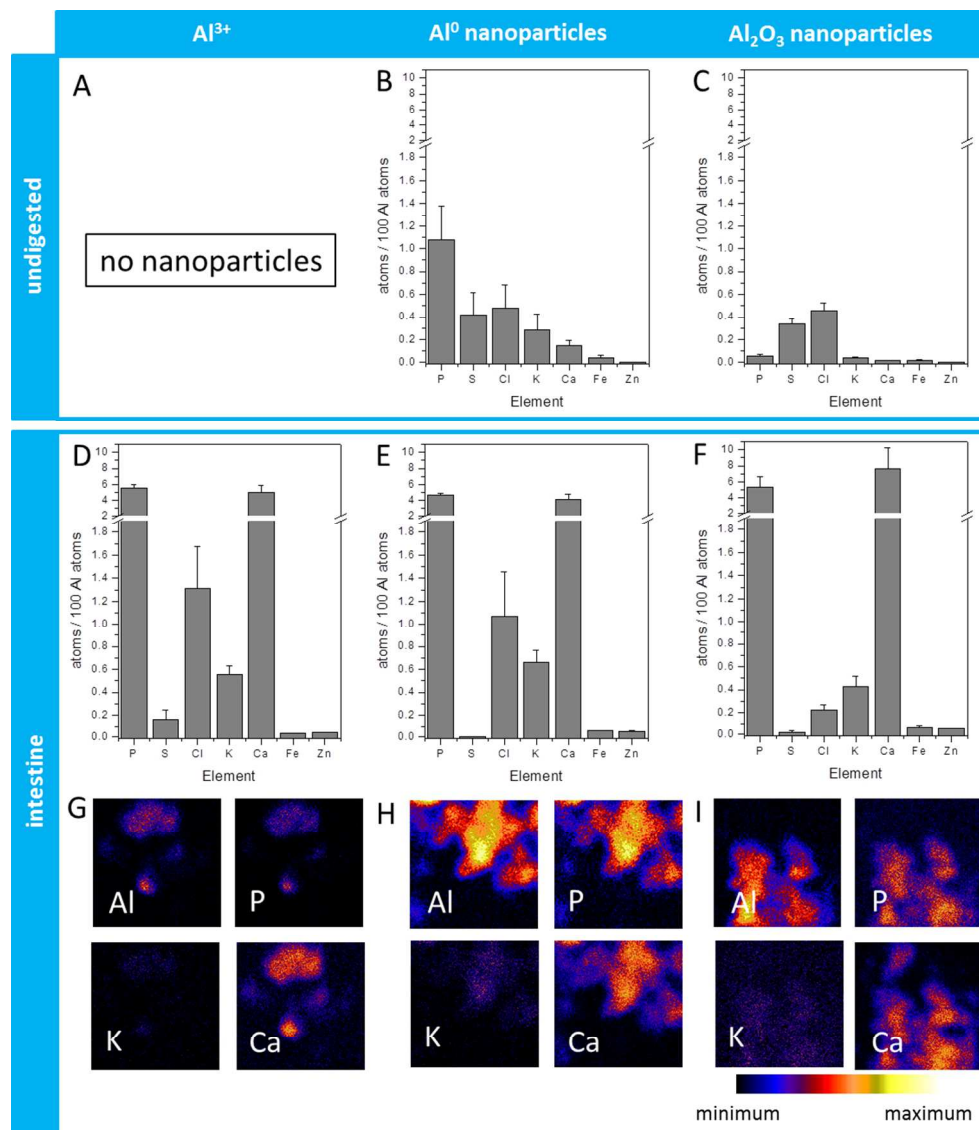


Figure 7: Digestion impact on surface modification of nanoparticles. (A - F): Element analysis of Al, of Al₂O₃ and de novo emerged particles resulted from AlCl₃. Samples were prepared following standard dispersion (A - C) as well as in intestinal fluid after having performed the full artificial digestion protocol (D - F). Each sample was measured at least 3 times on different positions. Error bars represent the standard deviation of the mean values. (G - I): μ PIXE images of element distributions in Al species after artificial digestion process. All images displaying an area of 25 x 25 μ m². The color code is as follow: minimal concentration is displayed black, while maximum is shown as white.

306x345mm (96 x 96 DPI)

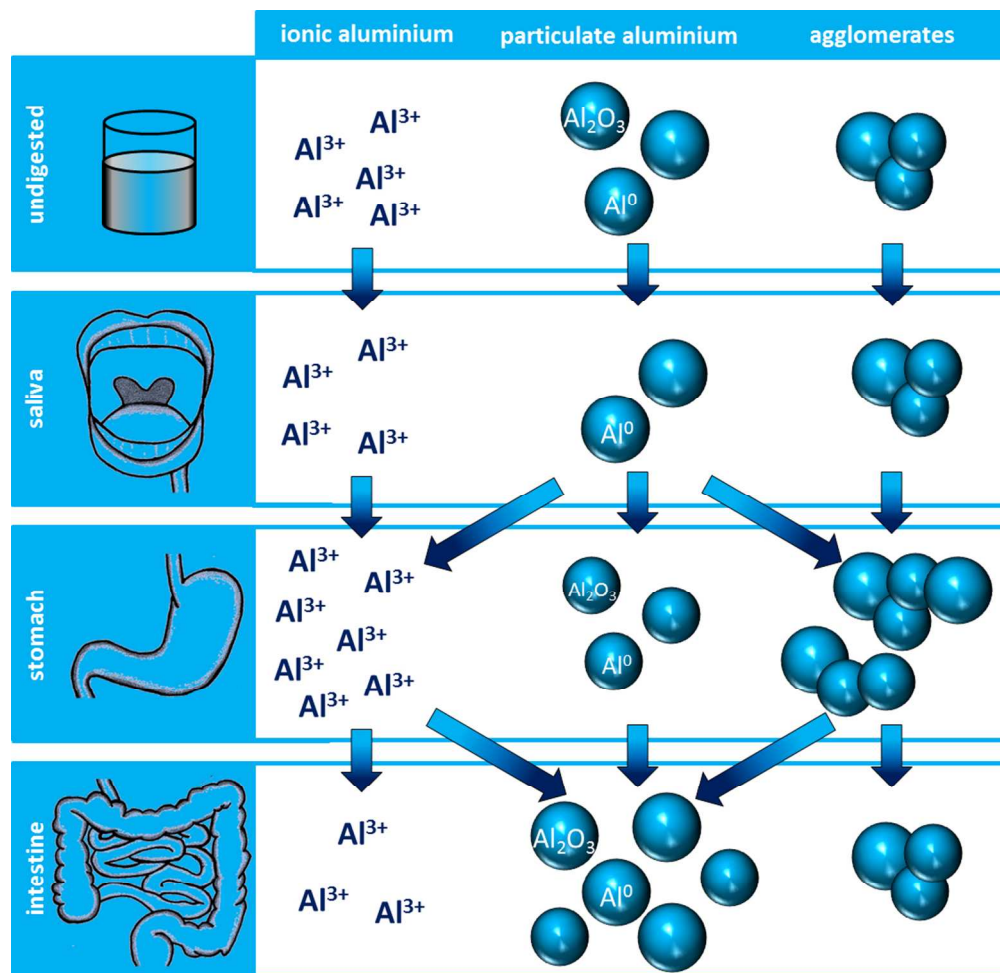
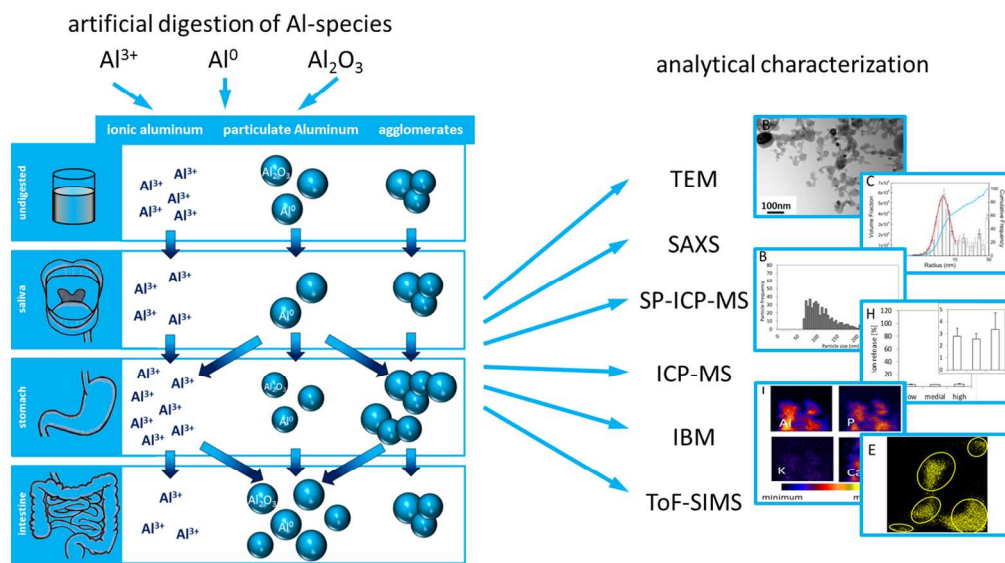


Figure 8: Suggested scheme of aluminum particle dissolution and agglomeration during the artificial digestion process. Samples stay unaffected in artificial saliva but agglomerate in the stomach fluid. At the same time, ions are released from particles but incomplete dissolution occurs. In intestinal fluid, agglomerates tend to de-agglomerate into primary particles and free ions form nano-scaled particulate structures, too.

299x290mm (96 x 96 DPI)



TOC

388x219mm (96 x 96 DPI)